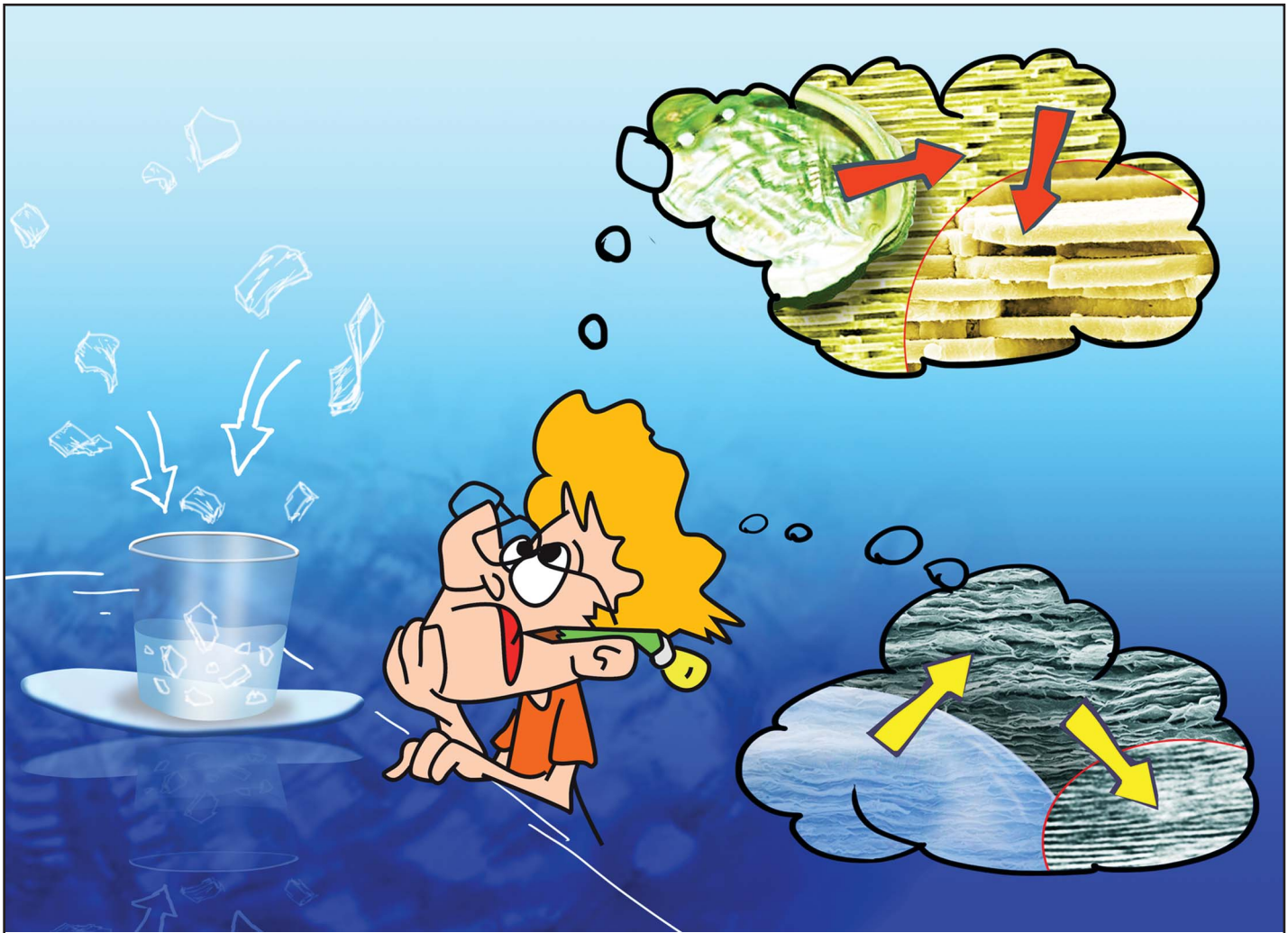

Showcasing research from the Key Laboratory of Bio-inspired Smart Interfacial Science and Technology, School of Chemistry and Environment, BeiHang University, Beijing, P. R. China.

Title: Understanding the relationship of performance with nanofiller content in the biomimetic layered nanocomposites

The cover picture illustrates the whole process of the researcher preparing the biomimetic layered nanocomposites inspired by natural nacre. These biomimetic nanocomposites show excellent mechanical properties and a hierarchical micro-/nano-scale structure. This novel biomimetic strategy brings a new concept for fabricating high performance layered nanocomposites for practical applications.

As featured in:

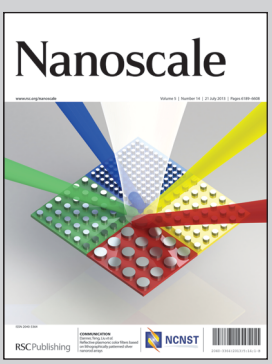

See Cheng *et al.*, *Nanoscale*, 2013, **5**, 6356.

RSC Publishing

www.rsc.org/nanoscale

Registered Charity Number 207890

Nanoscale

RSC Publishing

PAPER

View Article Online
View Journal | View Issue

Cite this: *Nanoscale*, 2013, **5**, 6356

Understanding the relationship of performance with nanofiller content in the biomimetic layered nanocomposites†

Jianfeng Wang,[a] Qunfeng Cheng,*[a] Ling Lin,[c] Linfeng Chen[b] and Lei Jiang[ab]

Montmorillonite/poly(vinyl alcohol) (MMT/PVA) nanocomposites spanning the complete range of MMT content (0–100 wt%) are prepared by simple evaporation-induced assembly. Effects of MMT content on the structure and mechanical properties of nanocomposites are systematically investigated and exhibit two important transitions at MMT contents of 30 wt% and 70 wt%. In the range of 0–30 wt%, the nanocomposites show a random structure. With the content of PVA increasing, the mechanical properties of the resultant nanocomposites were dramatically enhanced and were higher than that by prediction according to the conventional composite model. In the range of 30–70 wt%, the nanocomposites show a nacre-like layered structure with alternating MMT platelets and PVA layers, and all PVA is completely restricted by MMT platelets. The mechanical properties of nanocomposites were further improved by increasing the content of MMT, and reached the maximum value at the MMT content of 70 wt%. The 70 wt% MMT/PVA nanocomposite has a tensile strength of 219 ± 19 MPa, which is 5.5 times higher than that of a pure PVA film and surpasses nacre and reported biomimetic layered clay/PVA composites. When the MMT content is higher than 70 wt%, the layered structure is transformed to tactoids, which deteriorate mechanical properties. These results offer comprehensive understanding for developing high-performance biomimetic layered nanocomposite materials with high nanofiller loading.

Received 14th February 2013
Accepted 13th April 2013

DOI: 10.1039/c3nr00801k

www.rsc.org/nanoscale

Introduction

Nanofillers with outstanding mechanical properties, large specific surface area and aspect ratio, including carbon nanotubes, clay, and graphene, have been widely used to reinforce polymers to fabricate the nanocomposites.[1–4] Through optimization of the dispersion and interface chemistry, low-volume additions (1–10 vol%) of nanoparticles often provide marked property enhancements that are comparable to those achieved by high-volume additions (15–40 vol%) of traditional micrometer-scale fillers. Theoretically, the properties can be further improved by increasing the amount of nanofillers. However, the desired high-volume additions of nanofillers often result in structural inhomogeneities and deteriorate the performance. Through development of well-organized structure and robust interface, nature has created various nanocomposites with high inorganic component content and excellent mechanical properties, such as bone (~40 vol%), dentin (~45 vol%), enamel (~85 vol%), sponge spicule (~89 vol%) and nacre (~95 vol%).[5] Nacre, mother-of-pearl, in particular has attracted much attention.[6,7] The extremely high-volume incorporation of $CaCO_3$ platelets into a biopolymer matrix in the form of fantastic brick-and-mortar arrangement leads to a unique combination of remarkable strength, modulus and toughness.[8] Inspired by the brick-and-mortar structure and excellent mechanical properties of nacre, high-loading platelet-reinforced polymer composites have been fabricated by some assembly techniques,[9–11] including layer-by-layer (LBL) assembly,[12–17] air–water interface assembly technique,[18,19] ice-template assembly process,[20,21] electrophoretic deposition,[22,23] vacuum filtration assembly.[24–27] They displayed impressive mechanical properties, which were commonly attributed to high nanoplatelet content, compact layered structure and robust inorganic–organic interface. In order to develop high-performance nanocomposites for practical application, it is crucial to fully understand the effect of nanofiller loading on structure and mechanical properties. However, exact nanoplatelet loading in layered composites was difficult to control discretionarily in these previous works.

Herein, we report the preparation of biomimetic nacre-like montmorillonite/poly(vinyl alcohol) (MMT/PVA) nanocomposites

[a]*Key Laboratory of Bio-inspired Smart Interfacial Science and Technology of Ministry of Education, School of Chemistry and Environment, BeiHang University, Beijing, China. E-mail: cheng@buaa.edu.cn; Fax: +86-10-82627566*

[b]*Beijing National Laboratory for Molecular Sciences (BNLMS), Key Laboratory of Organic Solids, Institute of Chemistry, Chinese Academy of Sciences, Beijing, China*

[c]*Engineering Research Center of Marine Biological Resource Comprehensive Utilization, SOA, The Third Institute of Oceanography of the State Oceanic Administration, Xiamen, China*

† Electronic supplementary information (ESI) available. See DOI: 10.1039/c3nr00801k

via the water-evaporation-induced assembly technique.[28–32] The preparation process is simple and easy to be scaled up, compared with previously reported fabrication techniques, such as LBL, vacuum filtration, ice-template and other assembly techniques. The MMT content is regulated conveniently between 0 and 100 wt%. The dependence of structure and mechanical properties on MMT content exhibits two transitions. One is structure transition from random to nacre-like layered arrangement, corresponding to the change of mechanical properties from rapid increase to relatively slow increase. The other is structure transition from nacre-like layered arrangement to tactoids, corresponding to the change of mechanical properties from increase to decrease. These results offer comprehensive understanding for further developing high-performance biomimetic layered nanocomposite materials with high nanofiller loading for practical application.

Experimental section

Materials

PVA (M_w = 146 000–186 000; hydrolysis = 99 wt%) was purchased from sigma-Aldrich. MMT, which is Na^+-type montmorillonite was supplied by Zhejiang Fenghong Clay Co. Ltd. and used as received without further purification. High-purity and deionised MilliQ water was used in all experiments.

Preparation of MMT/PVA nanocomposites

A 0.6 wt% clay dispersion was prepared by dispersing as-received MMT (6 g) in water (1 L) under thorough stirring for one week and then centrifuged twice at 3000 rpm for 10 min to remove unexfoliated MMT. After centrifugation, the collected supernatant solution became transparent, with virtually no precipitation of clay platelet aggregates in one week. It was weighed, dried and re-weighed to determine MMT mass concentration. The concentration of the fine MMT suspension is typically 0.31 wt%. PVA powder was dissolved in water at 95 °C under slow stirring to form an aqueous solution (0.5 wt%). A desired amount of the PVA solution was gradually added to a stirred MMT dispersion. After that, the mixture was continually stirred for about 6 h at room temperature to maximize polymer adsorption and ensure fine dispersion of the stabilized clay platelets. Finally, this homogeneous MMT/PVA solution was poured into a culture dish and kept at room temperature for film formation until its weight equilibrated. It took about 4 days for generating a film with thickness of 7–9 μm. This film was easily peeled off from the bottom of the dish. A series of MMT/PVA composite films with different MMT weight fractions (0–100 wt%) were prepared by altering the mass ratio of MMT dispersion to PVA solution.

Characterization

The scanning electron microscopy (SEM) images were obtained with a field emission scanning electron microscope (S-4800, Hitachi) at an acceleration voltage of 5 kV. The acceleration voltage was increased to 10 kV for the energy-dispersive X-ray (EDX) measurements. Transmission electron microscopy (TEM) was performed using a JEOL JEM-2100 instrument at 200 kV. X-ray diffraction (XRD) experiments were carried out with a D/max-2500 (Rigaku) instrument using Cu-Kα radiation. Thermal gravimetric analysis (TGA) was conducted on a TG/DTA 6300 (SII Nano technology Inc., Japan) thermal analyzer at a heating rate of 10 °C min^{-1} under air. The thermal behavior of the films was further investigated *via* differential scanning calorimetry (DSC) using a DSC 6220 (SII Nano Technology Inc., Japan) instrument at a heating rate of 5 °C min^{-1} under N_2. Atomic force microscope (AFM) images were acquired using a Veeco Multimode VIII AFM. Dynamic light scattering (DLS) was performed using a light-scattering system (Dybapro NanoStar, Wyatt) at 25 °C at a scattering angle of 90°. The mechanical properties were measured in the tensile mode in a universal mechanical testing machine (Shimadzu AGS-X, Japan). The tested rectangular strips were about 50 mm in length and 3 mm in width. The distance between the clamps was 10 mm and the load speed was 0.5 mm min^{-1}. The exact cross-section widths and thicknesses were carefully determined by SEM. Light transmittance spectra of the films were measured using a Hitachi U-4100 UV-vis spectrophotometer.

Results and discussion

The preparation process first involves preparation of a fine colloidal dispersion containing discrete MMT nanoplatelets, as proved by AFM and DLS (Fig. S1 and S2, ESI†).[33–35] Then the dispersion was mixed with a dilute PVA solution at various ratios, followed by slow evaporation. To avoid the phase separation during evaporation, the polymer should strongly interact with MMT. Here, PVA was selected because a thin layer of PVA molecules can be tightly adsorbed onto a MMT platelet surface during mixing through hydrogen bond and covalent bond formation.[36] The modification prevented the MMT platelets from being re-aggregated in the process of evaporation. The resultant films are visually uniform and glossy. High transparency is basically maintained for MMT contents up to 70 wt% (Fig. S3, ESI†).

Morphology structure of nanocomposites

The effect of MMT content on the microstructures of composites was examined by SEM, as shown in Fig. 1. For low MMT concentrations, it can be observed that the MMT platelets are homogeneously embedded into the PVA matrix without obvious oriented arrangement (Fig. 1a). In contrast, a layered structure like that of nacre appears when the MMT concentration surpasses 30 wt% (Fig. 1b–f). The sheet-like layers are parallel to the film surface and interpenetrate into adjacent layers. This phenomenon also appeared in biomimetic clay–polymer composite films made by LBL assembly.[37] The state of dispersion of MMT in composites was further characterized by XRD (Fig. S4, ESI†). The majority of MMT is exfoliated for low MMT concentrations, while an intercalated layered structure is formed when the MMT concentration is between 30 wt% and 70 wt%. However, the structure of composites with more than 70 wt% MMT is transformed to tactoids.

It is well known that nanoparticles tend to congregate in nanocomposites with high filler content. Here, the distribution

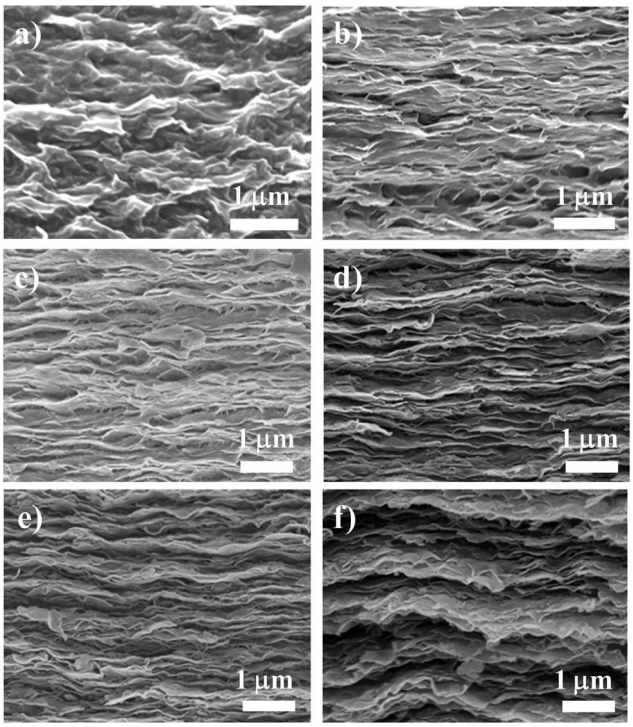

Fig. 1 SEM images of the cross-section. (a) 10 wt% MMT/PVA, (b) 30 wt% MMT/PVA, (c) 50 wt% MMT/PVA, (d) 70 wt% MMT/PVA, (e) 90 wt% MMT/PVA, and (f) 100 wt% MMT film. These show that a well-defined layered structure can be observed when the MMT loading is higher than 30 wt%.

of MMT was characterized by EDX and TEM. The MMT/PVA composite with loading of MMT up to 70 wt% was selected as the sample and shows homogeneous micro-/nanostructure. The full EDX spectrum of the cross-section exhibits the signals originating from PVA (carbon and oxygen) and MMT (sodium, magnesium, aluminium, silicon and oxygen) (Fig. 2b). The corresponding element mapping indicates the uniform distribution of MMT and PVA in the composite with such high nanofiller loading (Fig. S5, ESI†). A TEM image reveals highly aligned self-assemblies of alternating MMT nanoplatelets and PVA layers, similar to the films made by vacuum filtration assembly (Fig. 2c).[26] The grey scale analysis of TEM images shows a densitometric profile (Fig. 2d).[34,38] It reveals a gap of MMT platelets in the range of 1.7–2.1 nm. This spacing is consistent with the results from XRD.

The self-orientation of anisotropic nanoplatelets in polymers during evaporation has been reported, including clay and graphene.[28,29,39–41] It appears that a layered structure can be formed if the following requirements are met: (1) low viscosity of dispersion, (2) high platelet/polymer ratio and (3) slow evaporation rate. In our MMT/PVA system, the average aspect ratio of MMT is about 93. For all composites, the low viscosity of initial dispersion and slow evaporation at room temperature are basically the same, while the MMT/PVA ratio varies from zero to infinity. Hence, the morphological structure change is primarily ascribed to the difference of MMT/PVA ratios and can be explained by dynamics and thermodynamics.[40] For low ratio of platelets to polymer, the slow dynamics of polymer chains during evaporation traps MMT platelets apart, and thus they remain exfoliated in the polymer matrix. The kinetic constraint becomes weaker as the ratio of platelets to polymer increases. As a result, for high MMT/polymer weight ratios, the excluded-volume interactions between clay platelets induce the rearrangement into a layered structure for minimizing free energy of the system.[42]

Interfacial interaction

The interfacial interaction and the influence of MMT content on the crystallinity of PVA were investigated by DSC (Fig. S6, ESI†). Pure PVA shows a well-defined melting peak at ~225.5 °C. For composites, the melting peak signals sharply weaken with MMT concentration and the degree of crystallinity shows a significant decrease (Table S1, ESI†). The sharp weakening is due to the confinement of polymer chains by MMT with enormous specific

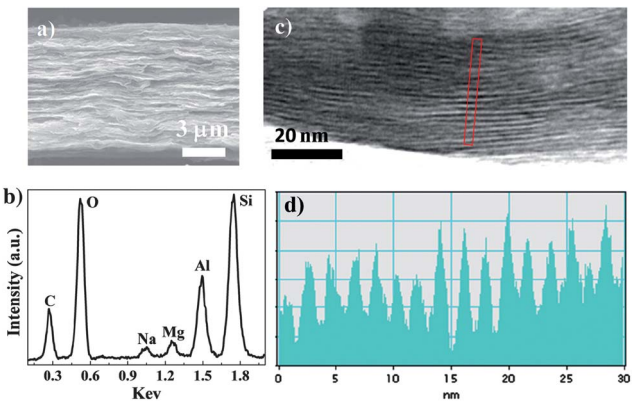

Fig. 2 (a) SEM image of the cross-section of a 70 wt% MMT/PVA composite. (b) The corresponding full EDX spectrum with all elements of MMT and PVA. (c) The TEM image showing the alternating hard and soft layers. (d) The grey scale analysis of the section marked in (c), revealing that the average spacing of MMT platelets is about 1.9 nm.

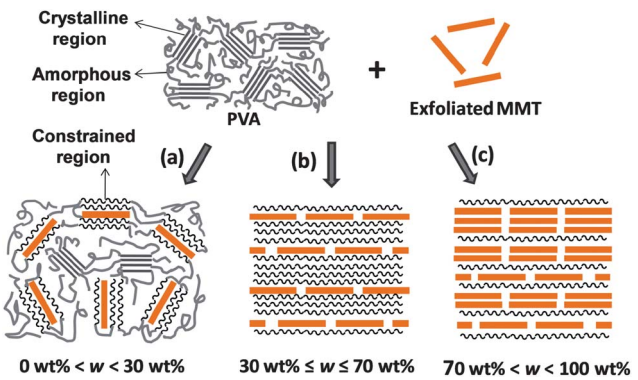

Scheme 1 Proposed structural models of MMT/PVA nanocomposites prepared by evaporation-induced assembly. (a) The composites with MMT weight fraction, *w*, between 0 wt% and 30 wt% have a random structure. The crystallinity of PVA decreases, accompanied by the increase of the constrained region. (b) The composites with *w* between 30 wt% and 70 wt% have a nacre-like layered structure. PVA is completely constrained by MMT platelets. (c) The structure of composites with *w* between 70 wt% and 100 wt% is transformed to tactoids.

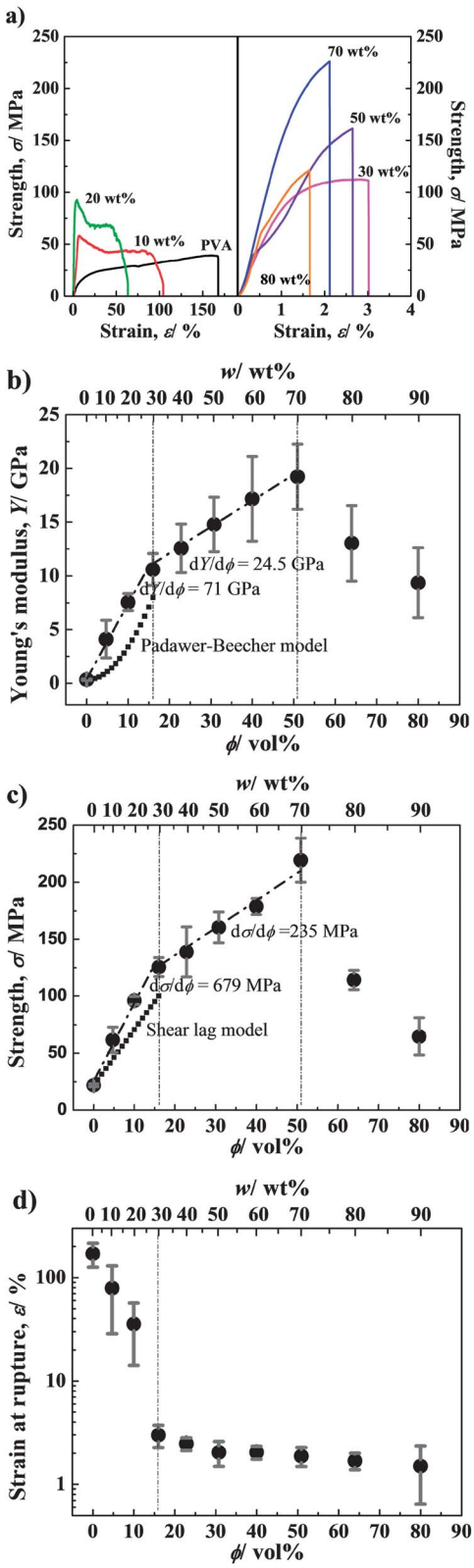

Fig. 3 Tensile testing results of MMT/PVA nanocomposites as a function of MMT content. (a) Representative stress–strain curves of MMT/PVA composites with different weight fractions of MMT. (b–d) The effect of MMT volume fraction, ϕ, on Young's modulus, strength and strain at rupture. The volume fraction was calculated by using the MMT weight fraction, w, and the densities of PVA and MMT. According to the change of Young's modulus, strength and strain at break, the MMT volume fraction can be divided into three regions: 0–16 vol%, 16–51 vol%, and 51–100 vol%. The acclivitous dashed lines represent linear fits to the corresponding volume fraction regime. The black-filled circles in (b) and (c) represent the predicted Young's modulus from the Padawer–Beecher model and the predicted strength from the shear lag model, respectively.

ratio area (~700 m^2 g^{-1}).[14,43] This implies strong interfacial interaction and effective stiffening of the affected PVA. The affected PVA forms an interphase zone. Moreover, the fraction of interphase PVA increases with MMT content. When the MMT content exceeds 30 wt%, the melting peak signal is completely suppressed. This indicates that a critical platelet fraction exists at which all of the polymer chains are affected and become interfacial. If we take the disappearance of the melting peak as the starting point when all of the PVA becomes interfacial, it can be inferred that the critical platelet weight fraction is about 30 wt%. In addition, incorporation of MMT enhances thermal stability of the polymer (Fig. S7, ESI†). The onset decomposition temperature of composites increases with MMT content. A considerable increase of 45 °C is found for a 60 wt% MMT/PVA composite. The improvement of thermal stability may be due to the constrained movement of polymer chains and reduced permeability of the nanocomposites.[44,45]

According to the morphology structure and interfacial interaction, the structural models of MMT/PVA nanocomposites are proposed, as shown in Scheme 1.

Mechanical properties

Besides the arrangement of MMT and crystallinity of the PVA matrix, MMT content has a great effect on the mechanical performance of composites. Typical stress–strain curves of composites are presented in Fig. 3a. Pure PVA has an initial elastic deformation followed by a large plastic deformation, with a tensile strength of 39.4 ± 0.8 MPa. The Young's modulus, yield strength and strain at break are about 0.34 GPa, 22 MPa and 170%, respectively. Upon incorporation of MMT, a well-defined yield point appears for 10 wt% and 20 wt% MMT/PVA composites. The yield strength enhances notably with the clay content. When the clay content surpasses 30 wt%, the composites fail at obviously lower strains. The strength is further improved, and no yield and plastic deformation are observed. Conversely, the strength abruptly falls as the MMT weight fraction is higher than 70 wt%. For a pure MMT film, no data could be obtained because it was too brittle to be tensile tested.

Based on the above-mentioned structure and interface analysis, we attempt to clarify the effect of the MMT content on mechanical performance of composites in the round. The effect can be quantified by the rate of increase of Young's modulus and strength with the volume fraction of MMT. The weight fraction of MMT is transformed into volume fraction, ϕ (Table S1, ESI†). The Young's modulus, strength and strain at rupture as a function of MMT volume fraction are obtained, as shown in Fig. 3b–d. In terms of the evolvement of Young's modulus, strength and strain at break, the MMT volume fraction is divided into three regions: 0–16 vol% (0–30 wt%), 16–51 vol% (30–70 wt%) and 51–100 vol% (70–100 wt%).

In the region of 0–16 vol%, the Young's modulus of composites increases sharply and reaches a much larger extent compared with conventionally filled polymer systems containing micron-sized fillers.[46,47] The rate of increase of the Young's modulus with ϕ, $dY/d\phi$, reaches about 71 GPa (Fig. 3b). Only 4.7 vol% addition of MMT increases the Young's modulus by 12.3 times, compared with that of pure PVA. A comparison of the results with those expected from the Padawer–Beecher model shows that the experimental Young's modulus is much larger than the theoretical prediction (see the ESI†).[48] A possible reason for larger Young's modulus than the theoretically predicted values is the MMT-induced PVA interfacial phase, which has a much higher modulus than the bulk equivalent polymer phase.[49] Moreover, the fraction of the interphase PVA enhances with MMT content. The similar interphase reinforcement phenomenon for nanocomposites is rare but reported in other literature.[50,51] The strength also increases dramatically with ϕ and the $d\sigma/d\phi$ reaches 679 MPa (Fig. 3c). Only 4.7 vol% addition of MMT increases the yield strength by 2.8 times. Again, the experimental values are larger than the theoretical predictions from the shear lag model (see ESI†).[52] Similar to the Young's modulus, the dramatic enhancement of strength is ascribed to both the increase of MMT platelet content and induced PVA interfacial phase. As expected, the strain at break decreases with ϕ (Fig. 3d). The remnant of the bulk-like PVA phase proved by DSC allows plastic deformations of the composites.

For the region of 16–51 vol%, the Young's modulus and strength linearly increase with no deterioration as ϕ increases, due to the ordered layered structure. Differently, the dependence of Young's modulus and strength on ϕ is weaker, compared with that in the region of 0–16 vol%. The $dY/d\phi$ and $d\sigma/d\phi$ are about 24.5 GPa and 235 MPa, respectively (Fig. 3b and c). The MMT content surpasses the critical platelet fraction, and all of the PVA chains in the composites are stiffened by clay platelets. It can be considered that, as the MMT content increases, the additional exfoliated MMT platelets are introduced into the polymer region that has already been affected by other MMT platelets. In other words, increasing clay content does not change the fraction of the interphase polymer. Thus, the rate of enhancement of Young's modulus and strength is slower than that in the first region. Surprisingly, the strength and Young's modulus reach 219 ± 19 MPa and 19.3 ± 3 GPa, respectively, at 51 vol% MMT. These values represent 5.5-fold and 57-fold increase, respectively, compared to those of pure PVA. The strength is larger than that of nacre (σ = 80–135 MPa).[8,53]

Fig. 4 summarizes the mechanical properties of our layered MMT/PVA composite and other reported layered clay/PVA composites prepared by LBL, vacuum filtration and doctor-blading assembly. It is evident that, besides superior modulus, the strength outperforms other biomimetic layered clay/PVA composites without crosslinks. The slow evaporation is a spontaneous process and finally reaches a balanced state, which has minimum free energy and is free of internal stress. This is probably responsible for higher mechanical properties. The comparison of the mechanical properties indicates that evaporation-induced assembly is also an effective method to prepare nacre-inspired layered nanocomposites with high performance. Comparison of preparation methods of nacre-inspired layered nanocomposites is shown in Table 1. Although it can precisely control over a layered structure, LBL assembly is laborious, time-consuming and hard to be scaled up. Because of the loss of the polymer during filtration, vacuum filtration assembly cannot exactly control the content of clay platelets.[25] The doctor-blading assembly is simple and fast, but the mechanical properties of the obtained composite are inferior, due to the weak control over the layered structure.[36] Comparatively, the evaporation-induced assembly method is simple, economic, easy to be scaled up and suitable for fabrication of a large-area sample. Furthermore, the content of clay platelets can be simply regulated. It is noted that the dispersion has to be highly stable. Although long, time consumption is probably reduced by suitably increasing the concentration of dispersion and evaporation temperature.

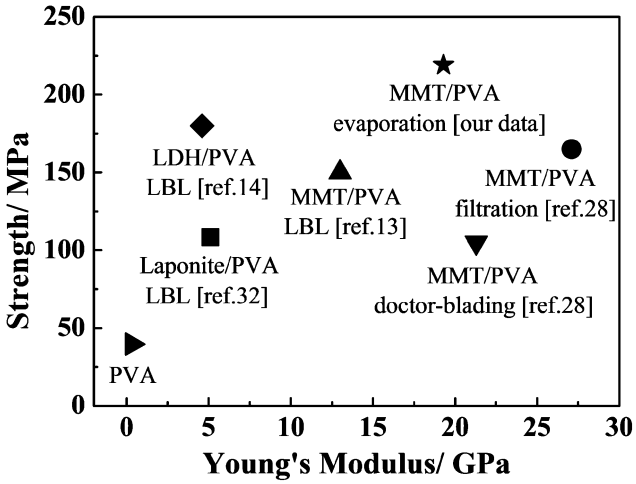

Fig. 4 Strength *vs.* Young's modulus of our nacre-like MMT/PVA composites compared with other layered clay/PVA composites.

As for deformation ability in the region of 16–51 vol%, the complete absence of the bulk-like PVA phase makes the composites brittle and finally, only two percentiles of ultimate strain are displayed (Fig. 3d). It should be point out that, although containing extremely high filler content, nacre still displays a plastic deformation accompanied by hardening after

Table 1 Comparison of preparation methods of biomimetic layered nanocomposites

Assembly	Advantages	Disadvantages
LBL	Fine control of structure	Laborious, time-consuming and hard to be scaled up
Doctor-blading	Simple and fast	Weak control of structure Low performance
Filtration	Can be scaled up	Hard to regulate platelet content
Evaporation	Economical, simple Easy to be scaled up and regulate platelet content High performance	Time-consuming High requirement for the stability of the dispersion

yield.[54] The plastic deformation of nacre was explained by wide slide of inorganic platelets over a large volume, which was believed to be controlled by aragonite bridges, nanoasperities, waviness of aragonite platelets and the stretching of an interfacial coiled biopolymer.[55] It is implied that, although effective for high modulus and strength, the simple layered structure is insufficient for excellent toughness.

In the region of 51–100 vol%, the strength and Young's modulus of composites turn to decrease with ϕ (Fig. 3b and c). It was reported that MMT platelets, which are only 1 nm in thickness, could directly absorb about 0.5 nm-thick polymer layers on each side, resulting in 50 vol% MMT/polymer nanocomposites.[36,56] Hence, for our system with more than 51 vol% MMT, it can be reasonably inferred that partial MMT platelets were not covered with PVA during mixing, due to the insufficiency of PVA. As a result, agglomerated tactoids were formed in the process of drying. This is confirmed by XRD in Fig. S4.† The restack tactoids lead to the degraded mechanical properties. These imply that a highest loading of MMT exists at which all nanoplatelets are just covered with one thin polymer layer. Obviously, the highest loading is limited by the thickness of nanoplatelets.

Conclusions

In summary, MMT/PVA nanocomposites with a full composition range of clay (0–100 wt%) were prepared by very simple evaporation-induced assembly. Low-loading additions (0–30 wt%) of MMT generate random structure and marked enhancement of mechanical properties that go beyond the expectation from the conventional composite theory, due to the unique interphase reinforcement mechanism. For high-loading additions (30–70 wt%), the random structure is transformed to a nacre-like layered structure, corresponding to further improvements of strength and Young's modulus in the form of a relatively slow rate. A highest clay content of 70 wt% limited by the nanoplatelet thickness exists, at which the Young's modulus and strength of the composite reach 19.3 ± 3 GPa and 219 ± 19 MPa, respectively. They are 57 times and 5.5 times those of pure PVA and partly surpass those of nacre. When clay loading exceeds the highest value, the nacre-like layered structure is transformed to tactoids, which inevitably lower the performance. The facile fabrication process and thorough elucidation of the relationship of structure and performance with nanoplatelet content would promote the development of biomimetic layered nanocomposites. Further direction for developing high-loading platelet-reinforced polymer composites should include the increase of extensibility. Due to complete restriction of a nanometer-thick polymer layer in between parallel platelets, nacre-like molecule-level toughening by stretching of coiled macromolecule chains is not available. Based on the layered structure, mimicking nacre's other toughening mechanisms may be possible.

Acknowledgements

This work was supported by the National Research Fund for Fundamental Key Projects (2010CB934700), the National Natural Science Foundation of China (21273017, 51103004), the Research Fund for the Doctoral Program of Higher Education (20101102120044), the Fundamental Research Funds for the Central Universities (YWF-12-LXGY-017), Program for New Century Excellent Talents in University (NCET-12-0034), Beijing Nova Program (Z121103002512020), Beijing Science and Technology Program (Z121100001312004), Innovation Foundation of BUAA for PhD Graduates, the Key Research Program of the Chinese Academy of Sciences (KJZD-EW-M01).

Notes and references

1 J. N. Coleman, U. Khan, W. J. Blau and Y. K. Gun'ko, *Carbon*, 2006, **44**, 1624–1652.
2 T. Kuilla, S. Bhadra, D. Yao, N. H. Kim, S. Bose and J. H. Lee, *Prog. Polym. Sci.*, 2010, **35**, 1350–1375.
3 S. Pavlidou and C. D. Papaspyrides, *Prog. Polym. Sci.*, 2008, **33**, 1119–1198.
4 P. May, U. Khan, A. O'Neill and J. N. Coleman, *J. Mater. Chem.*, 2012, **22**, 1278–1282.
5 M. A. Meyers, P.-Y. Chen, A. Y.-M. Lin and Y. Seki, *Prog. Mater. Sci.*, 2008, **53**, 1–206.
6 G. M. Luz and J. F. Mano, *Philos. Trans. R. Soc., A*, 2009, **367**, 1587–1605.
7 F. Barthelat, *Philos. Trans. R. Soc., A*, 2007, **365**, 2907–2919.
8 A. P. Jackson, J. F. V. Vincent and R. M. Turner, *Proc. R. Soc. London, Ser. B*, 1988, **234**, 415–440.
9 J. Wang, Q. Cheng and Z. Tang, *Chem. Soc. Rev.*, 2012, **41**, 1111–1129.
10 H.-B. Yao, H.-Y. Fang, X.-H. Wang and S.-H. Yu, *Chem. Soc. Rev.*, 2011, **40**, 3764–3785.
11 Q. Cheng, M. Li, L. Jiang and Z. Tang, *Adv. Mater.*, 2012, **24**, 1838–1843.
12 P. Podsiadlo, B. S. Shim and N. A. Kotov, *Coord. Chem. Rev.*, 2009, **253**, 2835–2851.
13 Z. Tang, N. A. Kotov, S. Magonov and B. Ozturk, *Nat. Mater.*, 2003, **2**, 413–418.
14 P. Podsiadlo, A. K. Kaushik, E. M. Arruda, A. M. Waas, B. S. Shim, J. Xu, H. Nandivada, B. G. Pumplin, J. Lahann, A. Ramamoorthy and N. A. Kotov, *Science*, 2007, **318**, 80–83.
15 J. B. Han, Y. B. Dou, D. P. Yan, J. Ma, M. Wei, D. G. Evans and X. Duan, *Chem. Commun.*, 2011, **47**, 5274–5276.
16 M. A. Priolo, D. Gamboa, K. M. Holder and J. C. Grunlan, *Nano Lett.*, 2010, **10**, 4970–4974.
17 M. A. Priolo, K. M. Holder, S. M. Greenlee and J. C. Grunlan, *ACS Appl. Mater. Interfaces*, 2012, **4**, 5529–5533.
18 L. J. Bonderer, A. R. Studart and L. J. Gauckler, *Science*, 2008, **319**, 1069–1073.
19 H.-B. Yao, H.-Y. Fang, Z.-H. Tan, L.-H. Wu and S.-H. Yu, *Angew. Chem., Int. Ed.*, 2010, **49**, 2140–2145.
20 S. Deville, E. Saiz, R. K. Nalla and A. P. Tomsia, *Science*, 2006, **311**, 515–518.
21 E. Munch, M. E. Launey, D. H. Alsem, E. Saiz, A. P. Tomsia and R. O. Ritchie, *Science*, 2008, **322**, 1516–1520.
22 T.-H. Lin, W.-H. Huang, I.-K. Jun and P. Jiang, *Chem. Mater.*, 2009, **21**, 2039–2044.

23 T.-H. Lin, W.-H. Huang, I.-K. Jun and P. Jiang, *Electrochem. Commun.*, 2009, **11**, 14–17.
24 A. Liu, A. Walther, O. Ikkala, L. Belova and L. A. Berglund, *Biomacromolecules*, 2011, **12**, 633–641.
25 K. W. Putz, O. C. Compton, M. J. Palmeri, S. T. Nguyen and L. C. Brinson, *Adv. Funct. Mater.*, 2010, **20**, 3322–3329.
26 A. Walther, I. Bjurhager, J.-M. Malho, J. Ruokolainen, L. Berglund and O. Ikkala, *Angew. Chem., Int. Ed.*, 2010, **49**, 6448–6453.
27 Q. Cheng, M. Wu, M. Li, L. Jiang and Z. Tang, *Angew. Chem., Int. Ed.*, 2013, 3750–3755.
28 T. Ebina and F. Mizukami, *Adv. Mater.*, 2007, **19**, 2450–2453.
29 N. Yousefi, M. M. Gudarzi, Q. Zheng, S. H. Aboutalebi, F. Sharif and J.-K. Kim, *J. Mater. Chem.*, 2012, **22**, 12709–12717.
30 A. E. Rawlings, J. P. Bramble and S. S. Staniland, *Soft Matter*, 2012, **8**, 6675–6679.
31 A. E. Rawlings, J. P. Bramble and S. S. Staniland, *Soft Matter*, 2013, **9**, 2341–2342.
32 M. Drack and I. C. Gebeshuber, *Soft Matter*, 2013, **9**, 2338–2340.
33 H. J. Ploehn and C. Liu, *Ind. Eng. Chem. Res.*, 2006, **45**, 7025–7034.
34 K. Kolman, W. Steffen, G. Bugla-Płoskońska, A. Skwara, J. Pigłowski, H.-J. Butt and A. Kiersnowski, *J. Colloid Interface Sci.*, 2012, **374**, 135–140.
35 M. Anyfantakis, A. Bourlinos, D. Vlassopoulos, G. Fytas, E. Giannelis and S. K. Kumar, *Soft Matter*, 2009, **5**, 4256–4265.
36 A. Walther, I. Bjurhager, J.-M. Malho, J. Pere, J. Ruokolainen, L. A. Berglund and O. Ikkala, *Nano Lett.*, 2010, **10**, 2742–2748.
37 P. Podsiadlo, A. K. Kaushik, B. S. Shim, A. Agarwal, Z. Tang, A. M. Waas, E. M. Arruda and N. A. Kotov, *J. Phys. Chem. B*, 2008, **112**, 14359–14363.
38 A. Kiersnowski, K. Kolman, I. Lieberwirth, S. Yordanov, H.-J. Butt, M. R. Hansen and S. H. Anastasiadis, *Soft Matter*, 2013, **9**, 2291–2301.
39 M. Zabska, K. Jaskiewicz, A. Kiersnowski, K. Szustakiewicz, S. Rathgeber and J. Piglowski, *Radiat. Phys. Chem.*, 2011, **80**, 1125–1128.
40 K. E. Strawhecker and E. Manias, *Chem. Mater.*, 2000, **12**, 2943–2949.
41 N. Ogata, S. Kawakage and T. Ogihara, *J. Appl. Polym. Sci.*, 1997, **66**, 573–581.
42 V. V. Ginzburg and A. C. Balazs, *Macromolecules*, 1999, **32**, 5681–5688.
43 T. U. Patro and H. D. Wagner, *Nanotechnology*, 2011, **22**, 455706.
44 S. Bourbigot, J. W. Gilman and C. A. Wilkie, *Polym. Degrad. Stab.*, 2004, **84**, 483–492.
45 S. Sinha Ray and M. Okamoto, *Prog. Polym. Sci.*, 2003, **28**, 1539–1641.
46 E. P. Giannelis, R. Krishnamoorti and E. Manias, *Adv. Polym. Sci.*, 1999, **138**, 107–147.
47 T. D. Fornes and D. R. Paul, *Polymer*, 2003, **44**, 4993–5013.
48 G. E. Padawer and N. Beecher, *Polym. Eng. Sci.*, 1970, **10**, 185–192.
49 D. Shia, C. Y. Hui, S. D. Burnside and E. P. Giannelis, *Polym. Compos.*, 1998, **19**, 608–617.
50 A. Eitan, F. T. Fisher, R. Andrews, L. C. Brinson and L. S. Schadler, *Compos. Sci. Technol.*, 2006, **66**, 1162–1173.
51 K. Hu, M. K. Gupta, D. D. Kulkarni and V. V. Tsukruk, *Adv. Mater.*, 2013, **25**, 2301–2307.
52 B. Glavinchevski and M. Piggott, *J. Mater. Sci.*, 1973, **8**, 1373–1382.
53 F. Barthelat, C.-M. Li, C. Comi and H. D. Espinosa, *J. Mater. Res.*, 2006, **21**, 1977–1986.
54 F. Barthelat, H. Tang, P. D. Zavattieri, C. M. Li and H. D. Espinosa, *J. Mech. Phys. Solids*, 2007, **55**, 306–337.
55 H. D. Espinosa, J. E. Rim, F. Barthelat and M. J. Buehler, *Prog. Mater. Sci.*, 2009, **54**, 1059–1100.
56 H.-B. Yao, Z.-H. Tan, H.-Y. Fang and S.-H. Yu, *Angew. Chem., Int. Ed.*, 2010, **49**, 10127–10131.

